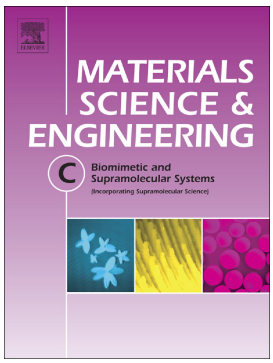

Comparative study of transdermal drug delivery systems of resveratrol: High efficiency of deformable liposomes

Maira Gaspar Tosato, Julie V. Maya Girón, Airton A. Martin, Vamshi Krishna Tippavajhala, Mónica Fernández Lorenzo de Mele, Lelia Dicelio

PII: S0928-4931(18)31061-0
DOI: doi:10.1016/j.msec.2018.04.073
Reference: MSC 8530

To appear in: *Materials Science & Engineering C*

Received date: 17 August 2017
Revised date: 12 April 2018
Accepted date: 25 April 2018

Please cite this article as: Maira Gaspar Tosato, Julie V. Maya Girón, Airton A. Martin, Vamshi Krishna Tippavajhala, Mónica Fernández Lorenzo de Mele, Lelia Dicelio , Comparative study of transdermal drug delivery systems of resveratrol: High efficiency of deformable liposomes. The address for the corresponding author was captured as affiliation for all authors. Please check if appropriate. Msc(2017), doi:10.1016/j.msec.2018.04.073

COMPARATIVE STUDY OF TRANSDERMAL DRUG DELIVERY SYSTEMS OF RESVERATROL: HIGH EFFICIENCY OF DEFORMABLE LIPOSOMES

Maira Gaspar Tosato[1*], Julie V. Maya Girón[1], Airton A. Martin[2], Vamshi Krishna Tippavajhala[3], Mónica Fernández Lorenzo de Mele[1] and Lelia Dicelio[4].

[1] The Research Institute of Theoretical and Applied Physical Chemistry (INIFTA), Universidad Nacional de La Plata, Calle 64 Diag. 113, 1900- La Plata, Buenos Aires, Argentina

[2] Biomedical Engineering Innovation Center, Biomedical Vibrational Spectroscopy Group, Universidade Brasil-UNBr, Rua Carolina Fonseca, 235-08230-030, Itaquera, Sao Paulo, Brazil and Visiting Professor, Departmento de Física, Universidade Federal do Piaui (UFPI), Campus Ministro Petronio Portella, Teresina, CEP: 64049-550, PI, Brazil.

[3] Department of Pharmaceutics, Manipal College of Pharmaceutical Sciences, Manipal University, Manipal, Karnataka, Pincode-576104, India.

[4] Universidad de Buenos Aires-INQUIMAE, Ciudad Universitaria, 1428- Buenos Aires- Argentina

[*]Corresponding author: Photosensitization and Molecular Photobiology Research Group, Research Institute of Theoretical and Applied Physical Chemistry (INIFTA) - Diag. 113 y calle 64 (1900)- La Plata, Buenos Aires, Argentina. Tel. +54(221) 4257430, int. 153;

Email address: mairagtosato@gmail.com

ABSTRACT

Trans-resveratrol (3, 5, 4' trihydroxystilbene, RSV) is a natural compound that shows antioxidant, cardioprotective, anti-inflammatory and anticancer properties. The transdermal, painless application of RSV is an attractive option to other administration routes owing to its several advantages like avoiding gastrointestinal problems and first pass metabolism. However, its therapeutic potential is limited by its low solubility and low stability in water and the reduced permeability of stratum corneum. To overcome these inconveniences the encapsulation of this

compound in a drug delivery system is proposed here. In order to find the best carrier for transdermal application of RSV various liposomal nanoparticulate carriers like conventional liposomes (L-RSV), deformable liposomes (LD-RSV), ultradeformable liposomes (LUD-RSV) and ethosomes (Etho-RSV) were assayed. Transmission electron microscopic (TEM) and dynamic light scattering (DLS) studies were performed to analyze the surface morphology of these carriers. Structural characterization for these formulations was performed by confocal Raman spectroscopy. The spectroscopic results were analysed in conjunction with calorimetric data to identify the conformational changes and stability of formulations in the different nanoparticles induced by the presence of RSV.

Comparison of the results obtained with the different carrier systems (L-RSV, LD-RSV, LUD-RSV and Etho-RSV) revealed that the best RSV carrier was LD-RSV. The increase in the fluidity of the bilayers in the region of the hydrophobic chains of the phospholipid by ethanol probably facilitates the accommodation of the RSV in the bilayer and contributes to the improved encapsulation of RSV without affecting the mobility of this carrier.

Keywords: Resveratrol; Transdermal drug delivery; Liposomes; Nanoparticles; Confocal Raman spectroscopy.

1. INTRODUCTION

Resveratrol (3, 5, 4' trihydroxystilben, RSV) is the main compound of stilbene phytoalexins which was first isolated from the roots of *Polygonum cuspidatum.* RSV is mainly found in peanuts, grapes and red wine [1][2] and exhibits interesting medical properties. The therapeutic potential of this compound is related to its antioxidant, cardioprotective, anti-inflammatory and anticancer ability properties [3][4][5] found specially in trans-RSV, more biologically active than the *cis* isomer [6]. Moreover, epidemiological studies showed an inverse correlation between red wine consumption and the incidence of cardiovascular disease [7].

Transdermal, painless application of RSV is an attractive option to other administration routes to avoid gastrointestinal problems and first pass metabolism [8]. However, RSV therapeutic potential of this route is limited by the reduced permeability of stratum corneum which is the main obstruction for the drug transport. Besides, RSV solubility is low (0.03 g/L) and its stability in water is deficient due to photoisomerization that reduces RSV activity. These limitations could be resolved through encapsulation of RSV in novel drug delivery systems. Novel strategies to increase the permeation and thereby the absorption of drugs through the skin such as vesicles (liposomes) [9], nanoparticles [10][11] and nanodroplets [12] have been proposed for several compounds of medical interest. Among these strategies, vesicular drug delivery systems based on liposomes have been extensively studied as possible carriers of other compounds because of its similarity to cell membranes, biocompatibility and low toxicity. However, it has been reported that conventional liposomes would not be suitable as transdermal drug delivery systems as they do not penetrate into deeper regions of skin and are retained in the upper layers of the stratum corneum [13][14]. Accordingly, new strategies are focused in the synthesis of novel drug delivery systems that can penetrate into these depths of skin such as deformable lipid vesicles (elastic and ultraflexible), known as deformable liposomes or transferosomes [15][16]. Several studies have reported that these deformable liposomes have exhibited improved effectiveness in the *in vitro* release of hydrocortisone, dexamethasone and methotrexate and ability to penetrate into the deeper layers of skin, achieving the delivery of the actives to their therapeutic levels [17][18]. Delivery is facilitated by the osmotic gradient between the inner and outer layer of the stratum corneum [19] and by the flexibility and elasticity of these transferosomes that make their transport through the spaces between the cells that comprise the stratum corneum easier. This ability is not found in the traditional liposomes [20].

Other novel vesicular drug delivery systems called ethosomes, developed by Touitou have also gained relevance in the last decade [13][21]. Ethosomes are noninvasive lipid vesicles containing high concentrations of ethanol which promote their penetration through the skin. This property makes them interesting as vehicles for topical drug delivery. Comparing with conventional liposomes or hydro alcohol solutions, the ethosomes diffuse more efficiently into the skin tissue due to its flexibility and malleability, improving drug delivery into deep layers such as the dermis and reaching the circulatory system [16][22]. Under high concentrations of ethanol the lipid membrane turns loose making the stratum corneum a soft structure with greater capacity for the distribution of drugs without decreasing the its stability [23][24].

All in all, various liposomal nanoparticulate carriers for RSV like conventional liposomes (L-RSV), deformable liposomes (LD-RSV), ultradeformable liposomes (LUD-RSV) and ethosomes (Etho-RSV) were assayed. Comparison of the results obtained with the different carrier systems were made in order to select the best alternative for transdermal application of RSV. To the best of our knowledge this is the first time that the comparison of four different liposomes for transdermal release of RSV is reported and the more appropriate is selected with the aim of resolving the low permeability of RSV in the stratum corneum. With this purpose, size distribution, polydispersity index, surface morphology and encapsulation efficiency of the nano-carriers were evaluated. Transmission electron microscopic (TEM) and dynamic light scattering (DLS) studies were also performed to analyze their surface morphology. Additionally, structural characterization was achieved by confocal Raman spectroscopy. The spectroscopic results were complemented with calorimetric data to identify the conformational changes and stability of formulations in the different nanoparticles induced by the presence of RSV.

2. MATERIALS AND METHODS

2.1 Materials

Soy phosphatidylcholine (Phospholipon® 90G, PL90) was purchased from Lipomize (Argentina - Lipoid GmbH, Ludwigshafen, Germany). Tween 80, chloroform and ethanol were purchased from Merck (Germany). Resveratrol (Shaanxi Berries Biochemical Co, Ltda, RSV) was a gift from Elisium (Capital Federal, Buenos Aires, Argentina).

2.2 Aqueous solution of RSV

RSV has low solubility in water. It was solubilized by magnetic agitation for 1h at 27°C in darkness. Samples were protected from the light during preparation and were stored in an amber colored glass bottle to avoid photodegradation. The concentration of resveratrol studied was 65 µM at pH 6.5±0.1.

2.3 Preparation of carriers

Suspensions were prepared by film method. Lipids and drug were dissolved in chloroform (10 mL) and the organic solvent was removed by rotary evaporation (Büchi Rotavapor R-114) in a water bath at 40 °C (Büchi Waterbath B-480) and 70 cm Hg. Deposited lipid film was hydrated with Milli Q water by rotation. Suspensions were filtered three times through 450 µm Millipore. Incorporation of RSV in these systems was performed in the solvent because of its better solubility when compared with water. The samples were prepared in triplicate. Vials were kept refrigerated until the moment of analysis.

2.3.1 Conventional liposomes (L and L-RSV)

5 mg of RSV was dissolved in chloroform (10 mL) and mixed with 0.11 g of PL90. The solution was evaporated to form a thin film and was hydrated with 10 mL of Milli Q water. This was followed by 90 min agitation at room temperature to obtain large multilamellar vesicles. The mixture was divided into conical tubes and sonication for 2 min to obtain a translucent dispersion. The same procedure was followed in the preparation of blank liposomes without RSV (control, L).

2.3.2 Deformable liposomes (LD and LD-RSV)

15 mg of RSV was dissolved in chloroform and the PL90/Tween80 (1:4) mixture was added and mixed (LD-RSV). Film hydration was obtained with water: ethanol (7% v/v) and agitated for 1h at 39 ºC. The mixture was kept at rest for 2 hours to attain full hydration. Similarly, the blank deformable liposomes were prepared without RSV and used as control (LD).

2.3.3 Ultradeformable liposomes (LUD and LUD-RSV)

Ultradeformable liposomes were formulated with PL90, Tween 80 and cholesterol. The PL90 and cholesterol (11:1) mixture was dissolved in chloroform. RSV was dissolved in chloroform before mixing with lipids (LUDRSV). To these films, 10 mL of water and Tween 80 (0.026 g) were

added and stirred for 1 h. Similar procedure was used in the preparation of blank ultradeformable liposomes without RSV which was used as control (LUD).

2.3.4 Ethosomes (Etho and Etho-RSV)

19 mg of RSV was dissolved in ethanol (3 mL) and 0.42 g of lipid was added to the drug solution. 7 mL of Milli Q water was added slowly in a fine stream to the above mixture with constant mixing at 750 rpm for 30 min at 35 ºC (EthoRSV). Samples were kept at rest for 2 h and then sonicated for 2 min. The control sample was prepared using same procedure without RSV (Etho).

2.4 Characterization

2.4.1 UV-visible spectroscopy

Aqueous RSV solution was scanned and the spectral absorbance was recorded in the range of 200-500 nm using a Shimadzu UV-Vis-NIR 3600 spectrophotometer with a 1 cm path length quartz cell (Figure S1, Supplementary information)

2.4.2 Dynamic Light Scattering (DLS)

Different dilutions for each of these suspensions were prepared in aqueous medium at room temperature. The particle sizes, polydispersity index (PI) and size distribution of these formulations were measured using a particle size analyzer (90Plus/BI-MAS) with He-Ne laser (658 nm) and 15mW power. The average values were obtained from 3 measurements of 40 secs each one. A sample with a PI < 0.05 was considered as monodispersed [25].

2.4.3 Transmission Electron Microscopy (TEM)

The samples were diluted (1:10) and maintained refrigerated until the measurement. The samples on the grid were contrasted with uranyl acetate for duration of 20 secs. The morphology

of these various liposomes was examined using a JEOL 1200 EX II electron microscopic unit operated at 100 kV accelerating voltage (JEOL Ltd., Tokyo, Japan) and equipped with Erlangshen ES1000W (Gatan Inc., Pleasanton, California, USA) camera at Electronic Microscopy Center of Facultad de Ciencias Veterinarias (UNLP, Argentine).

2.4.4 Drug encapsulation efficiency of Resveratrol

Determination of free/unencapsulated RSV from these formulations was carried out by dialysis through semipermeable membrane (D9527, Sigma Aldrich). The release system was maintained under magnetic stirring (100 rpm) at room temperature and immersed in glass flasks containing 250 mL of water. An aliquot of 1 mL of RSV aqueous solution was monitored by UV-*vis* spectroscopy at different times (40, 60, 120, 180, 240, 300, 360 min and 21 h). Results of encapsulation efficiency (E %) were calculated using the following equation (equation 1) and were expressed as the mean ± standard deviation (SD) of released RSV. It was calculated using the absorbance values of these solutions in the wavelength (λ) of 305 nm.

$$E(\%) = \frac{C_I - C_F}{C_I} \cdot 100 \qquad (1)$$

where C_I is initial concentration and C_F is final concentration determined after dialysis. Experiments were performed at room temperature (27 °C) and at a pH of 6.5±0.1 [26]. Zupancic et al. [27] showed that RSV in aqueous solution was stable at room or body temperature at weakly acidic conditions of pH 6.8. Degradation of RSV is exponential above this pH value. The exposure to light and oxygen was avoided in order to maintain the stability of the *trans* isomer. The percentage of cumulative drug release (%CDR) profile of each delivery system was calculated. The graph is in the Supplementary Information (Figure S3).

2.4.5 Differential Scanning Calorimetry (DSC)

In this study, the effect of incorporation of RSV was investigated on the thermotropic behavior of lipid bilayers of different formulations. Calorimetric measurements were carried out by Shimadzu DSC-50 at a temperature range of -100 °C to 130 °C with 10 °C/min scanning speed. The maximum temperature of the transition endotherm (T_m) and the enthalpy (ΔH) were determined in the samples with and without RSV using N_2 atmosphere with a 30 mL/min flux.

2.4.6 Structural characterization by confocal Raman Spectroscopy

Confocal Raman analysis was performed using a Rivers Diagnostics spectrometer (3510 SCA model) with 785 nm excitation (25 mW). The spectral range studied was from 400 to 1800 cm^{-1} and 2700 to 3900 cm^{-1}. The integration time of each spectrum was 10 s. The background due to the fluorescence of the skin tissue was corrected using a polynomial baseline correction and smoothing functions appropriate for each range. The peak positions were determined using second derivatives and subsequent deconvolution of the spectra.

3. RESULTS AND DISCUSSION

3.1 TEM, DLS and DSC Characterization

The membrane stability of drug delivery systems generally depends on the composition, chemical structure and the nature of the encapsulated drug [27]. These factors may affect the permeability of the particles in biological environment, encapsulation of drugs and stability. The carriers loaded with RSV were characterized and compared with their controls through transmission electron microscopy (TEM), dynamic light scattering (DLS) and differential scanning calorimetry (DSC).

3.1.1 Transmission Electron Microscopy (TEM)

Figures 1 (a) and (b) show the images obtained for Etho and Etho-RSV. Spherical particles population were observed in both pictures. The arrows in Figure 1 (a) indicate broken structures

which seem to be a core and its bilayer environment. The average sizes of nanoparticles were similar, 136 ± 14 nm for Etho and 140 ±16 nm for Etho-RSV. Figures 1 (c) and (d) show images of TEM for deformable systems LD-RSV and LD, respectively. Both samples were spherical but show heterogeneity in size. LD-RSV nanoparticles are more spaced to each other when compared with LD samples. According to the images, the average sizes are smaller for LD, 83 ± 10 nm than for LD-RSV, 95 ± 12 nm and nanoparticles showing heterogeneity in size. Figures 1 (e) and (f) correspond to L and L-RSV. They show smaller nanoparticles for L but markedly larger for L-RSV (64.5 ± 14 nm and 176.5 ± 28 nm, respectively). Liposomes with RSV can be seen in a well-defined structure.

Images of ultradeformable particles, LUD show particles with average size equal to 86 ± 12 nm and, like L-RSV, LUD-RSV its size is almost double, 172,5 ± 27 nm, (Figure 1 (g) and (h)).

3.1.2 Dynamic Light Scattering (DLS)

The study of formulations reveals that the polydispersity index was less than 0.3 for all samples, with the exception of Etho. This sample presented a slightly higher value indicating that the particle population was relatively heterogeneous in size (Table 2). A larger size for Etho-RSV, L-RSV and LUD-RSV than their controls (without RSV) was observed due the presence of RSV. It could be explained by the presence of RSV located in the lipid bilayer. It could also be associated to the gradient between the external aqueous environment and RSV dissolved in the aqueous core of the nanoparticles driving water into these particles by osmosis and causing an increase in size which is similar to swelling of the red blood cells in hypotonic solution.

In the case of the deformable liposomes (LD and LD-RSV), both presented smaller sizes than other nanoparticles. This decrease can be related to the presence of ethanol which causes changes in the net charge of the system inducing steric stabilization which could lead to a decrease in the average size [30]. Ethanol content of ethosomes (30% v/v) is higher than LD systems (7% v/v), this influences positively on the mobility of the lipid bilayer. In addition, LD-RSV exhibits a size below 10 nm compared with LD. This formulation also showed higher encapsulation than all the others. Based on these results, it can be concluded that there are more nanoparticles in this system and consequently the encapsulation of RSV was higher.

3.1.3 Differential Scanning Calorimetry (DSC)

DSC analysis was performed to evaluate the effect of the incorporation of RSV on thermotropic behavior of lipid bilayers of nanoparticles. The transition temperature (T_m) and the enthalpy value (ΔH) were obtained for the samples with and without RSV. The measurements were made in the -75 °C to 75 °C temperature range and the scan range was 10 °C/min. A single endothermic peak was detected (Table 3).

Transition temperatures obtained for L and LUD showed no significant differences due to the incorporation of RSV, while, in the case of Etho and LD, the changes were 14.8° C and 3.11° C, respectively. It is known that at higher T_m values, the membrane acts as a fluid introducing some asymmetry in the hydrophobic part of the molecules. On the other hand, depending on the position of unsaturation in the hydrophobic portion, T_m may decrease [30]. Similar behaviour between nanoparticles when the values of phase transition enthalpy are obtained. Thus, the incorporation of RSV increased enthalpy values for LD-RSV and Etho-RSV. It is considered that the degree of order of lipids in the bilayers is reflected in the values of enthalpy. A lipid in asymmetric or amorphous state requires less energy than the ordered state to overcome the forces of cohesion [31]. Higher enthalpy values suggest that lipids have an orderly arrangement indicating a bilayer without major changes.

Based on the results shown in Table 3, the values corresponding to the ethosomes, which increase significantly in size after the addition of RSV, are in agreement with those obtained by DLS. This indicates that RSV molecules are in the ethanolic core of ethosomes and the interaction with the lipid bilayer is weak (higher values of ΔH and ΔS) and the bilayer remains orderly cohesive but with some fluidity due to ethanol (higher values of T_m) [32]. LD and LD-RSV present behaviour similar to that of ethosomes. No marked changes in L-RSV and LUD-RSV were observed due to the presence of RSV compared with the controls. In case of conventional liposomes, there is a decrease of 0.57 °C (ΔT_m) for the L-RSV while LUD-RSV exhibit an increase of 1.28 °C, related to the controls without RSV. This behavior may be associated with the low incorporation of RSV in such systems.

Overall, TEM and DLS techniques confirmed the formation of spherical nanoparticles. Results of sizes obtained by these two methodologies show differences that can be explained

taken into account the hydrodynamic ratio involved in the DLS measurements. DSC qualitative studies of the effect of RSV on the lipid bilayer of the nanoparticle revealed that RSV molecules can be found in the ethanolic nuclei in the EthoRSV, weakly interacting with the lipids of the bilayer, which remained orderly cohesive but with higher fluidity due to the presence of ethanol. The amount of ethanol used in the preparation of nanoparticles is enough for the formation of ethanolic nuclei and to promote a better fluidity of the lipid membrane without causing any disorder to the membrane. The changes in the T_m values of L-RSV and LUD-RSV were not pronounced, but express significant alterations in the bilayer due to the presence of RSV.

3.2 Structural characterization by confocal Raman spectroscopy

Trans-RSV molecule consists of two phenyl rings connected through an unsaturated double bond C=C with three hydroxyl groups in the rings. Considering the molecular vibrations of each group, the allocations to the peaks and Raman bands of RSV solution were made on the basis of theoretical knowledge and experimental data obtained from the various studies in the literature [33][34]. The molecular structure of RSV, with the numerical positions of atoms, was adapted from Vongsvivut [33] and it was utilized to describe the Raman vibrational modes where *p* is the position *para* (ring 1) and *m* is *meta* (ring 2) (Figure S2, Supplementary Information).

Although there are many studies in the literature relating the use of Raman spectroscopy to evaluate liposomes and derivatives, most of them are oriented to direct applications of nanoparticles in biological systems [35]–[38] and very few studies analyze the composition of nanoparticles using Raman spectroscopy [39], [40]. Figure 2 represents the Raman spectra in low frequency (400-1800 cm^{-1}) of Etho, Etho-RSV, L, L-RSV, LD, LD-RSV, LUD, LUD-RSV and aqueous solution of RSV (130 μM). This range is known as the fingerprint because it contains the main vibrational modes of the samples. The samples containing RSV were compared with the systems without RSV.

Two regions of the spectra were analysed: (I) 1125-1340 cm^{-1} and (II) 1545-1715 cm^{-1}. It is noted that LUD-RSV, Etho-RSV and LD-RSV samples exhibited significant spectral similarity in both regions. Considering the spectrum of the aqueous solution of RSV, both regions (grey bands) show

the characteristic contributions of RSV except L-RSV that did not show changes in relation to L. The spectra of the controls LUD, LD and Etho are extremely similar with L as exception.

In the regions I (1125-1340 cm^{-1}) and II (1545-1715 cm^{-1}) eight and four vibrational modes were analysed, respectively. According to Figure 2, intense bands were seen at 1607 and 1634 cm^{-1} for Etho-RSV, LD-RSV, and LUD-RSV and at 1633 cm^{-1} for L-RSV. Both bands were attributed to combinations of stretching vibrations, ν(C=C) and deformations, δ (=C–H) of the double bond linking ring 1 and 2 associated with vibrations of *para*-OH (O_p-H) of ring 1. The bands corresponding to 1603, 1627 and 1633 cm^{-1} are assigned to the spectrum of RSV solution. In the same region, there is a vibrational mode at 1656 cm^{-1} assigned to ν(C=C) of alkyl chains (apolar part) of phosphatidylcholine for formulations without RSV (Etho, LD, L and LUD) [40]. This vibrational mode is present in all spectra with RSV and displayed as a shoulder of the broadband, which also contains the peaks related to RSV. Similarly, peak 1588 cm^{-1} attributed to O-H deformation of the *p*-position was found in the formulations containing RSV except L-RSV. Moreover the wavenumber was constant and of higher intensity in all spectra when compared to the aqueous solution of RSV. These vibrational modes indicate the existence of an overlap between the vibrational modes of RSV and the modes related to the alkyl chains. Additionally in the spectrum of RSV solution, a triple band at 1154, 1169 and 1176 cm^{-1} can be distinguished It has been assigned to deformation vibration, δ(C–H) of ring 2 and δ(C–H) and δ(Op–H) of ring 1 associated with stretching ν(C10–C=) and ν(C–O) of ring 2.

Spectra of nanoparticles containing RSV show an overlap of the 1169 and 1176 cm^{-1} peaks that leads to a single band at 1172 cm^{-1}. In this region, no peaks related to vibrational modes of lipids were found. On the other hand, the spectra of nanoparticles without RSV, presented a characteristic peak at 1086 cm^{-1}, related to stretching vibrational modes, ν(C-C) of skeleton chain conformation *gauche* (indicative of a disorder of lipid chain). These vibrational modes are sensible to conformational state of the hydrocarbons chain [42]. In all spectra containing RSV, a decrease in the intensity value related to this peak was observed. However, Etho-RSV showed a peak at 1114 cm^{-1} which is also related to *gauche* band. These characteristics can be associated with the fluidity of the lipid bilayer of nanoparticles. Moreover, in LUD-RSV spectrum a peak at 1064 cm^{-1} can be differentiated. It is associated with C-C stretching in *trans* conformation indicating an orderly chain. The *gauche* conformation may be related to increased mobility of hydrocarbon backbone associated to unsaturation. According to the location of RSV in the system, the vibration with

gauche conformation can disappear or induce a reordering of the lipids. The contribution at 1207 cm^{-1} is attributed to stretching between the carbon atoms located in the 4 and 8 positions, ν(C4-C=) and indicates no significant change in all the spectra of the formulations with RSV except for L-RSV sample that presents a shift to 1215 cm^{-1}. Vibrational modes related to lipids in this region were not found in the spectra of the formulations without RSV. The absence of vibrational modes associated with RSV molecule in the L-RSV sample may be connected with the low encapsulation and/or the location of RSV in the carriers. 1304 and 1314 cm^{-1} peaks attributed to RSV may be related to the vibrational mode of twist of CH_2. This mode is found in the nanoparticles without RSV. In the presence of the compound, there is a sum of peaks that generates a wide band.

Figure 3 shows the Raman spectra of formulations in the high frequency range of 2700 to 3900 cm^{-1}. In this region, major modes related to lipid molecules and water are included. The spectral differences in this region were used to identify conformational behaviour of the lipids constituting the nanoparticles. The conformational changes of the lipids in the nanoparticles with and without RSV are indicated in the Figure 3 in a grey stripe.

Table 5 combines the band assignments according to the literature for the major peaks and changes in frequency values as a result of a structural change [33],[40][43]. The range comprised between 2850 and 3000 cm^{-1} is dominated by the presence of vibrations of ν(CH) associated with strong contributions of $\nu_{sym}CH_2$, $\nu_{asym}CH_2$ and harmonic binary interactions of δ (CH_2) due to the Fermi resonance [43]. The bands around 2850, 2877 and 2882 cm^{-1} are associated with symmetric stretching ν_{sym} (CH_2), ν_{sym} (CH_3) and asymmetric stretching ν_{asym} (CH_2) of lipid chains respectively. We observed CH_3 group stretching only in the LD-RSV sample. When this sample was compared with its control (LD), it was observed that the intensity of the peaks related to the lipids decreased in the presence of RSV and absorbance bands were shifted from 2852 and 2902 cm^{-1} (LD) to 2850 and 2908 cm^{-1} (LD-RSV). These characteristics may be related to the changes in lipid chains due to the presence of RSV either located in the bilayer or very close to these lipids.

Comparing the intensities of peaks in the range of 2850 and 2930 cm^{-1} between Etho and Etho-RSV formulations, a decrease was observed for the samples of Etho-RSV. For this same sample a 2882 cm^{-1} peak related to $\nu_{asym}(CH_2)$ disappeared and bands at 2902 cm^{-1} and 3012 cm^{-1} related to vibrational modes ν(CH) and ν_{asym}(=CH) respectively appeared. The band located at 3012 cm^{-1} is attributed unsaturated hydrocarbon chains stretching that are related to internal vibrations of the lipid tail and interactions between side chains [44][45]. The changes occurred in the

EthoRSV may be associated to RSV located in the bilayer because of the presence of molecules of ethanol that compose the bilayer. Three low intensity peaks related to lipids were observed in the spectrum of L sample. Surprisingly, no peaks related to the lipids or RSV was found in L-RSV sample. A possible explanation for this observation is that the interaction of RSV with the lipids produced a total shift of these peaks to the region of vibrational modes of the water located (2726 cm^{-1}). The peaks at 2850 and 2882 cm^{-1} were analysed to estimate the relative population of *trans* and *gauche* conformations of alkyl lipid chains. The decrease in the peak intensity assigned to ν_{asym} CH_2 (2882 cm^{-1}) of CH_2 is related to fewer *trans* conformations of lipid alkyl chains. Furthermore, a shift of 2850 cm^{-1} peak, ν_{sym} (CH_2), towards shorter wavelengths indicates an increase in the *trans* population [46][47]. Shift in the Raman spectrum of LD-RSV from 2852 cm^{-1} to 2850 cm^{-1} indicates an increase of lipid chain order confirming the results obtained in the low frequency region. However, the 2884 cm^{-1} peak (ν_{asym} CH_2) showed a significant decrease in its intensity. It is possible to have a mixture of ordered rearrangements between the chains as both these vibrational modes were observed in the samples containing RSV. These results clearly indicate that the presence of this compound influences the order of lipid bilayer in these nanoparticles.

All spectra considered, it is concluded that Raman spectroscopy served as a highly sensitive technique to detect conformational changes of nanoparticles due to the presence of RSV. In the low frequency region, the spectral changes owing to the presence of RSV in the nanoparticulate formulations can be clearly distinguished when compared with their respective controls (blank formulations). The fluidity of the bilayer increased maintaining the order was detected as a peak related to *gauche* conformation of the lipids in the Etho-RSV sample. These results were corroborated with those found in the DSC where the presence of ethanol in the bilayer promoted fluidity without disturbing the lipid chain. In the case of LUD-RSV spectral a change related to *trans* conformation was observed indicating the order of lipid chains. The presence of RSV may hide the appearance of the *gauche* conformation or may cause order in the lipids.

In the high frequency region assigned to vibrational modes of lipids significant changes were found in the solutions containing RSV. Alterations in the intensity and displacement in wavelengths were found in the Etho-RSV samples in the characteristic region of lipid conformation indicating that RSV could be located in the bilayer and also in the nuclei because of ethanol. The

results of LD-RSV were corroborated with the values found in low frequency region and calorimetry indicating the order of lipid bilayers.

3.3 Drug encapsulation efficiency

Absorbance spectra of aqueous solutions with 65µM concentration of *trans*-RSV indicated a characteristic band with peaks located in 305 and 317 nm. Hypsochromic effect was observed after 30 min of irradiation using the 370 nm lamp and 305 and 317 nm peaks (*trans* isomer) shifted to 287 and 316 nm (*cis* isomer), respectively were noticed [48]. Solutions were characterized in the 200-400 nm range where the main information about isomers of RSV is located. Furthermore, absorbance values decreased mainly at 317 nm peak that disappeared after irradiation.

RSV was released from vesicular systems using a dialysis membrane and was monitored through spectral absorption at 305 nm. After 40 min of dialysis, a characteristic band of RSV could be observed in all spectra. The release of RSV into the water from ethosomes and liposomes was greater than those of deformable and ultradeformable liposomes.

The encapsulation efficiency (E %) values, shown in Table 1, correspond to the % of RSV encapsulated in the systems related to the total drug content. The highest value was measured for LD-RSV, followed by Etho-RSV, L-RSV and LUD-RSV. This could be explained due to the presence of the surfactant Tween 80 and the adequate amount of ethanol in the composition of deformable vesicles. Kronberg et al. reported that liposomes containing surfactant exhibit greater E (%) than the liposomes without this compound [49]. The presence of Tween did not affect the mobility of the polar groups. Additionally, there was an increase in the fluidity of the bilayers in the region of the hydrophobic chains of the phospholipid [50], which may improve encapsulation of RSV. On the other hand, the higher efficiency may also be related to the stabilizing action of ethanol in carriers so that the higher concentration of ethanol might provide increased membrane fluidity facilitating drug accommodation in the bilayer and a consequent increase in the E (%). Jain et al. related the encapsulation efficiency with the amount of ethanol. They reported that the presence of ethanol concentrations above certain limit creates instability and damage to the lipid bilayer [51]. Consequently, it seems that another factor could be related to the high solubility of RSV in ethanol (approx. 50 mg/mL) and may partly account for the decrease in the value of E (%) found in the ethosomes compared with those obtained for the other systems. Thus, some RSV remains

dissolved in the ethanol / water mixture instead of being encapsulated in the ethosomes. The encapsulation effect of RSV was reflected in the size increase of nanoparticles observed by TEM microscopy and DLS. Etho-RSV incorporated 51% of RSV showing an increase of about 5% in the size compared with the control Etho. On the other hand, L-RSV and LUD-RSV with 23% and 12.6% of RSV encapsulated, respectively showed an increase in size of over 100%. LD-RSV showed 10% increase in the size even though the encapsulation efficiency was 91.8%. The capacity of encapsulation and the nanoparticles sizes are related to the characteristics of the lipid bilayers like their structure and the type of carrier formed.

4. CONCLUSIONS

In order to find the best carrier for transdermal application of RSV various liposomal nanoparticulate carriers like conventional liposomes (L-RSV), deformable liposomes (LD-RSV), ultradeformable liposomes (LUD-RSV) and ethosomes (Etho-RSV) were assayed and a comparative analysis of the results was made.

Results revealed that the best RSV carrier was LD-RSV. This could be explained due to the presence of the surfactant Tween 80 and the adequate amount of ethanol in the composition of deformable liposomes. The increase in the fluidity of the bilayers in the region of the hydrophobic chains of the phospholipid by ethanol probably facilitates the accommodation of the RSV in the bilayer and contributes to the improved encapsulation of RSV without affecting the mobility of the carrier. LD-RSV showed 10% increase in the size and 91.8% encapsulation efficiency. Other factors that contribute to the higher efficiency of LD-RSV than the other systems may be related to its adequate amount of ethanol that improves the solubility of RSV without damage or instability of the lipid bilayer.

Acknowledgements

The present work was supported by the Consejo Nacional de Investigaciones Científicas y Técnicas (CONICET) and Universidad de Buenos Aires (SECYT-UBA), Argentina. MFLM thanks ANPCyT, PICT 2016 – 1424 for the financial support. M.G.T thanks CONICET for doctoral research fellowship.

References

[1] R. F. Casper, M. Quesne, I. M. Rogers, T. Shirota, A. Jolivet, E. Milgrom, and J. F. Savouret, "Resveratrol has antagonist activity on the aryl hydrocarbon receptor: Implications for prevention of dioxin toxicity.," *Mol. Pharmacol.*, vol. 56, no. 4, pp. 784–790, 1999.

[2] P. Langcake and R. J. Pryce, "The production of resveratrol by Vitis vinifera and other members of the Vitaceae as a response to infection or injury," *Physiol. Plant Pathol.*, vol. 9, no. 1, pp. 77–86, 1976.

[3] J. K. Aluyen, Q. N. Ton, T. Tran, A. E. Yang, H. B. Gottlieb, and R. a Bellanger, “Resveratrol: potential as anticancer agent.,” *J. Diet. Suppl.*, vol. 9, no. 1, pp. 45–56, 2012.

[4] L. G. Carter, J. A. D’Orazio, and K. J. Pearson, “Resveratrol and cancer: Focus on in vivo evidence,” *Endocrine-Related Cancer*, vol. 21, no. 3. 2014.

[5] G. Singh and R. S. Pai, “Recent advances of resveratrol in nanostructured based delivery systems and in the management of HIV / AIDS,” *J. Control. Release*, vol. 194, pp. 178–188, 2014.

[6] L. Camont, C. H. Cottart, Y. Rhayem, V. Nivet-Antoine, R. Djelidi, F. Collin, J. L. Beaudeux, and D. Bonnefont-Rousselot, “Simple spectrophotometric assessment of the trans-/cis-resveratrol ratio in aqueous solutions,” *Anal. Chim. Acta*, vol. 634, no. 1, pp. 121–128, 2009.

[7] L. Frémont, “Biological effects of resveratrol,” *Antioxidants {&} redox Signal.* vol. 3, no. 6, pp. 1041–1064, 2001.

[8] G. M. El Maghraby and A. C. Williams, “Vesicular systems for delivering conventional small organic molecules and larger macromolecules to and through human skin,” *Expert Opin. Drug Deliv.* vol. 6, no. 2, pp. 149–163, 2009.

[9] T. M. Allen and P. R. Cullis, “Liposomal drug delivery systems: From concept to clinical applications,” *Adv. Drug Deliv. Rev.*, vol. 65, no. 1, pp. 36–48, 2013.

[10] V. Jenning, A. Gysler, M. Schäfer-Korting, and S. H. Gohla, “Vitamin A loaded solid lipid nanoparticles for topical use: Occlusive properties and drug targeting to the upper skin,” *Eur. J. Pharm. Biopharm.*, vol. 49, no. 3, pp. 211–218, 2000.

[11] H. Pinto-Alphandary, A. Andremont, and P. Couvreur, “Targeted delivery of antibiotics using liposomes and nanoparticles: Research and applications,” *International Journal of Antimicrobial Agents*, vol. 13, no. 3. pp. 155–168, 2000.

[12] M. Kreilgraad, “Application of a Pharmacokinetic Microdialysis Model to Assess Skin Penetration,” in *Cutaneous Drug Delivery Potential of Microemulsion Vehicles*, Kopenhagen: Royal Danish School of Pharmacy, 2000.

[13] E. Touitou, N. Dayan, L. Bergelson, B. Godin, and M. Eliaz, “Ethosomes - novel vesicular carriers for enhanced delivery: characterization and skin penetration properties,” *J. Control. Release*, vol. 65, no. 3, pp. 403–18, May 2000.

[14] M. M. a Elsayed, O. Y. Abdallah, V. F. Naggar, and N. M. Khalafallah, “Lipid vesicles for skin delivery of drugs: reviewing three decades of research.,” *Int. J. Pharm.*, vol. 332, no. 1–2, pp. 1–16, Mar. 2007.

[15] G. Cevc, “Transfersomes, liposomes and other lipid suspensions on the skin: permeation enhancement, vesicle penetration, and transdermal drug delivery,” *Crit. Rev. Ther. Drug Carrier Syst.*, vol. 13, no. 3–4, pp. 257–388, 1996.

[16] E. Touitou, “Drug delivery across the skin,” *Expert Opin Biol Ther*, vol. 2, no. 7, pp. 723–733, 2002.

[17] M. Trotta, E. Peira, M. E. Carlotti, and M. Gallarate, “Deformable liposomes for dermal administration of methotrexate,” *Int. J. Pharm.*, vol. 270, no. 1–2, pp. 119–125, 2004.

[18] G. Cevc and G. Blume, “Hydrocortisone and dexamethasone in very deformable drug carriers have increased biological potency, prolonged effect, and reduced therapeutic dosage,” *Biochim. Biophys. Acta – Biomembr.* vol. 1663, no. 1–2, pp. 61–73, 2004.

[19] G. Cevc and G. Blume, “Lipid vesicles penetrate into intact skin owing to the transdermal osmotic gradients and hydration force,” *BBA – Biomembr.* vol. 1104, no. 1, pp. 226–232, Mar. 1992.

[20] G. Cevc, A. Schätzlein, and H. Richardsen, “Ultradeformable lipid vesicles can penetrate the skin and other semi-permeable barriers unfragmented. Evidence from double label CLSM experiments and direct size measurements,” *Biochim. Biophys. Acta Biomembr.* vol. 1564, no. 1, pp. 21–30, 2002.

[21] B. Godin, E. Touitou, E. Rubinstein, A. Athamna, and M. Athamna, “A new approach for treatment of deep skin infections by an ethosomal antibiotic preparation: an in vivo study,” *J. Antimicrob. Chemother,* vol. 55, no. 6, pp. 989–94, Jun. 2005.

[22] G. M. M. El Maghraby, A. C. Williams, and B. W. Barry, “Skin delivery of oestradiol from lipid vesicles: Importance of liposome structure,” *Int. J. Pharm.*, vol. 204, no. 1–2, pp. 159–169, 2000.

[23] V. Meidan, F. Alhaique, and E. Touitou, “Vesicular carriers for topical delivery,” *Acta Technol. Legis Medicam.*, vol. 9, no. 1, pp. 1–6, 1998.

[24] P. Anitha, S. Ramkanth, and K. Sankari, “Ethosomes-A noninvasive vesicular carrier for transdermal drug delivery,” *Int J Rev Life Sci*, vol. 1, no. 1, pp. 17–24, 2011.

[25] V. A. Hackley and C. F. Ferraris, *The use of nomenclature in dispersion science and technology*, vol. 960, no. 3. US Department of Commerce, Technology Administration, National Institute of Standards and Technology, 2001.

[26] Zhou, Y. and Raphael, R.M., “Solution pH alters mechanical and electrical properties of phosphatidylcholine membranes: Relation between interfacial electrostatics, intramembrane potential, and bending elasticit”, *Biophysical Journal*, vol. 92 (7), pp. 2451–2462, 2007.

[27] Š. Zupančič, Z. Lavrič, and J. Kristl, “Stability and solubility of trans-resveratrol are strongly influenced by ph and temperature,” *Eur. J. Pharm. Biopharm.*, no. April, 2015.

[28] L. Villafuerte, B. García, M. de L. Garzón, A. Hernández, and M. L. Vázquez, “Nanopartículas lipídicas sólidas,” *Rev. Mex. Ciencias Farm.*, vol. 39, no. 1, pp. 38–52, 2008.

[29] D. D. Lasic, N. Weiner, M. Riaz, and F. Martin, “Liposomes,” *Sci. Med.*, vol. 3, pp. 34–43, 1996.

[30] C. Gregor, *Phospholipids Handbook*. Marcel Dekker, Inc, New York, 1993.

[31] D. Hou, C. Xie, K. Huang, and C. Zhu, “The production and characteristics of solid lipid nanoparticles (SLNs),” *Biomaterials*, vol. 24, no. 10, pp. 1781–1785, 2003.

[32] F. Postigo, M. Mora, M. a. De Madariaga, S. Nonell, and M. L. Sagristá, “Incorporation of hydrophobic porphyrins into liposomes: Characterization and structural requirements,” *Int. J. Pharm.*, vol. 278, no. 2, pp. 239–254, 2004.

[33] J. Vongsvivut, E. G. Robertson, and D. McNaughton, “Surface-Enhanced Raman Scattering Spectroscopy of Resveratrol,” *Aust. J. Chem.*, vol. 61, no. 12, pp. 921–929, 2008.

[34] F. Billes, I. Mohammed-Ziegler, H. Mikosch, and E. Tyihak, “Vibrational spectroscopy of resveratrol,” *Spectrochim. Acta - Part A Mol. Biomol. Spectrosc.* vol. 68, no. 3, pp. 669–679, 2007.

[35] M. Mélot, P. D. a Pudney, A.-M. Williamson, P. J. Caspers, A. Van Der Pol, and G. J. Puppels, “Studying the effectiveness of penetration enhancers to deliver retinol through the stratum cornum by in vivo confocal Raman spectroscopy,” *J. Control. Release*, vol. 138, no. 1, pp. 32–9, Aug. 2009.

[36] M. Förster, M.-A. Bolzinger, D. Ach, G. Montagnac, and S. Briançon, “Ingredients tracking of cosmetic formulations in the skin: a confocal Raman microscopy investigation,” *Pharm. Res.*, vol. 28, no. 4, pp. 858–72, Apr. 2011.

[37] L. Franzen, D. Selzer, J. W. Fluhr, U. F. Schaefer, and M. Windbergs, “Towards drug quantification in human skin with confocal Raman microscopy.,” *Eur. J. Pharm. Biopharm.*, vol. 84, no. 2, pp. 437–44, Jun. 2013.

[38] P. P. Shah, P. R. Desai, D. Channer, and M. Singh, “Enhanced skin permeation using polyarginine modified nanostructured lipid carriers,” *J. Control. Release*, vol. 161, no. 3, pp. 735–45, Aug. 2012.

[39] E. Kočišová, A. Antalik, and M. Prochazka, “Drop coating deposition Raman spectroscopy of liposomes: Role of cholesterol,” *Chem. Phys. Lipids*, vol. 172–173, pp. 1–5, 2013.

[40] T. J. O’Leary, P. D. Ross, and I. W. Levin, “Effects of anesthetic and nonanesthetic steroids on dipalmitoylphosphatidylcholine liposomes: a calorimetric and Raman spectroscopic investigation,” *Biochemistry*, vol. 23, no. 20, pp. 4636–41, 1984.

[41] E. Guillard, A. Tfayli, M. Manfait, and A. Baillet-Guffroy, “Thermal dependence of Raman descriptors of ceramides. Part II: Effect of chains lengths and head group structures,” *Anal. Bioanal. Chem.*, vol. 399, no. 3, pp. 1201–1213, 2011.

[42] Z. Movasaghi, S. Rehman, and I. U. Rehman, “Raman Spectroscopy of Biological Tissues,” *Appl. Spectrosc. Rev.*, vol. 42, no. 5, pp. 493–541, Sep. 2007.

[43] A. Tfayli, E. Guillard, M. Manfait, and A. Baillet-Guffroy, “Thermal dependence of Raman descriptors of ceramides. Part I: Effect of double bonds in hydrocarbon chains,” *Anal. Bioanal. Chem.*, vol. 397, no. 3, pp. 1281–1296, 2010.

[44] A. Percot and M. Lafleur, “Direct observation of domains in model stratum corneum lipid mixtures by Raman microspectroscopy,” *Biophys. J.*, vol. 81, no. 4, pp. 2144–2153, 2001.

[45] M. R. Bunow and I. W. Levin, “Molecular conformations of cerebrosides in bilayers determined by Raman spectroscopy,” *Biophys. J.*, vol. 32, no. 3, pp. 1007–21, 1980.

[46] R. Neubert, W. Rettig, S. Wartewig, M. Wegener, and a Wienhold, “Structure of stratum corneum lipids characterized by FT-Raman spectroscopy and DSC. II. Mixtures of ceramides and saturated fatty acids,” *Chem. Phys. Lipids*, vol. 89, no. 1, pp. 3–14, Sep. 1997.

[47] M. Wegener, R. Neubert, W. Rettig, and S. Wartewig, “Structure of stratum corneum lipids characterized by FT-Raman spectroscopy and DSC. III. Mixtures of ceramides and cholesterol,” *Chem. Phys. Lipids*, vol. 88, no. 1, pp. 73–82, Aug. 1997.

[48] D. A. Rodríguez, “Utilización de Señales Fluorescentes para el Análisis y Caracterización de Vinos. Mejora de la Sensibilidad y Selectividad Mediante Derivatización Fotoquimica,” Universidad de Extremadura, 2008.

[49] B. Kronberg, a Dahlman, J. Carlfors, J. Karlsson, and P. Artursson, “Preparation and evaluation of sterically stabilized liposomes: colloidal stability, serum stability, macrophage uptake, and toxicity.,” *J. Pharm. Sci.*, vol. 79, no. 8, pp. 667–71, 1990.

[50] T. Subongkot, N. Wonglertnirant, P. Songprakhon, T. Rojanarata, P. Opanasopit, and T. Ngawhirunpat, “Visualization of ultradeformable liposomes penetration pathways and their skin interaction by confocal laser scanning microscopy,” *Int. J. Pharm.*, vol. 441, no. 1–2, pp. 151–161, 2013.

[51] R. G. S. Maheshwari, R. K. Tekade, P. a. Sharma, G. Darwhekar, A. Tyagi, R. P. Patel, and D. K. Jain, “Ethosomes and ultradeformable liposomes for transdermal delivery of clotrimazole: A comparative assessment,” *Saudi Pharm. J.*, vol. 20, no. 2, pp. 161–170, 2012.

Legends of Figures

Figure 1. TEM images of carriers: (a) Etho, (b) Etho-RSV, (c) LD, (d) LD-RSV, (e) L, (f) L-RSV, (g) LUD, (h) LUD-RSV

Figure 2: Raman spectra of different liposomal formulations studied in the low frequencies.

Figure 3: Raman spectra of different liposomal formulations measured in high frequency region.

Table 1. Encapsulation efficiency in liposomal formulations

Formulation	Encapsulation efficiency (%)*
Etho-RSV	51.0
L-RSV	23.0
LD-RSV	91.8
LUD-RSV	12.6

Table 2. Size and polydispersity index for all liposomal formulations

Samples	*Nanoparticle size	*Polydispersity index
Etho	131.8 ± 1.6	0.33 ± 0.01
EthoRSV	289.6 ± 0.9	0.25 ± 0.005
LD	94.9 ± 1.9	0.29 ± 0.03
LDRSV	84.1 ± 1.0	0.28 ± 0.01
L	149.3 ± 2.9	0.29 ± 0.1
L-RSV	220.5 ± 2.2	0.22 ± 0.009
LUD	131.2 ± 2.5	0.29 ± 0.005
LUDRSV	201.3 ± 0.8	0.21 ± 0.03

*Data presented as mean ± SD (n=3)

Table 3. Thermodynamics parameters: Effect of RSV incorporated in the liposomes

Samples	T_m[a] (°C)	ΔH[b] (J g^{-1})	ΔS[c] (J g^{-1} K^{-1})
L	4.51	350	1.26
L-RSV	3.94	350	1.26
Etho	-1.04	120	0.46
Etho-RSV	3.74	340	1.23
LD	0.60	260	0.95
LD-RSV	3.71	340	1.23
LUD	3.54	340	1.23
LUD-RSV	4.82	350	1.26

[a]T_m: Temperature for the maximum value of calorimetric peak.

[b]ΔH: Calorimetric enthalpy calculated as area under the curve.

[c]ΔS: Calorimetric entropy calculated as $\Delta H/T_m$

Table 4. Wavenumbers (cm^{-1}) of Raman spectra and description of vibrational modes of the RSV in aqueous solution and liposomal nanoparticles [33][34]. Region I (1125-1340 cm^{-1}) and Region II (1545-1715 cm^{-1}) are analysed.

	Raman shift of the samples (cm^{-1})					Assignments[#]
	RSV	**Etho-RSV**	**LD-RSV**	**L-RSV**	**LUD-RSV**	
Region I	1153	1149	1149		1149	$\delta(C–H)_{ring2}$ + $\nu(C10–C=)$ + $\nu(C–O)_{ring2}$
	1169					$\delta(C–H)_{ring1}$ + $\delta(O_p–H)$
	1176	1172	1172		1172	$\delta(C5–H)_{ring1}$ + $\delta(O_p–H)$
	1207	1207	1208	1215	1208	$\nu(C4–C=)$ + $\delta(=C–H)$
	1262	1262	1265		1258	$\nu(C_p–C=)$ + $\delta(=C–H)$ + $\delta(O_m–H)$ +δ(C5-H) + δ(C15–H)
	1304	1302				$\delta(C–H)$ + $\delta(O_m–H)$
	1314	1316				$\delta(C–H)$
Re	1588	1587	1588		1587	$\nu(C=C)_{ring1}$ + $\delta(O_p–H)$

g i o n II	1603	1607	1607		1607	ν(C=C)+ δ(=C–H) + $\nu(C=C)_{rings}$ + δ(O–H)
	1627	1634	1635	1633	1635	ν(C=C)rings + δ(O–H)
	1633					ν(C=C)rings + δ(=C–H) + ν(C=C)rings

[#] ν: stretch; δ: in-plane deformation

Table 5. Raman band assignments of different liposomal formulations [34], [41]-[44]

	Samples								Assignments
	RSV	Etho	Etho-RSV	LD	LD-RSV	L	LUD	LUD-RSV	
Raman shift (cm^{-1})		2726				2726			ν(OH)
		2850	2850	2852	2850	2851	2852	2851	$\nu_{sym}(CH_2)$
					2877				$\nu_{sym}(CH_3)$
		2882		2884	2885	2897	2884	2894	$\nu_{asym}(CH_2)$
			2902	2902	2908				ν(CH)
		2932	2930	2934	2935	2932	2932	2932	$\nu(CH_3)$ + $\delta(CH_2)$
		2976		2978			2977		$\nu(CH_3)$ + cholesterol
	3002								ν(CH)
			3012	3010			3009		ν_{asym}(=CH)
	3056								ν(C6-H) + ν(C5-H) anti-phase

ν: stretch; ν_{asym}: asymmetric stretch; ν_{sym}: symmetric stretch; δ: deformation

Highlights

- Four transdermal drug delivery systems (DDS) of resveratrol (RSV) were assayed and characterized: Liposomes (L), deformable (LD), ultradeformable (LU) and ethosomes (Etho)
- The best DDS for RSV were deformable L (LD-RSV) with 91.8% encapsulation efficiency
- Tween 80 and the adequate amount of ethanol contribute to the improved encapsulation
- Ordered rearrangements between the lipids chains of LD were found after RSV adding

Graphical Abstract